energies

MDPI

Article

A High-Power Solar PV-fed TISO DC-DC Converter for Electric Vehicle Charging Applications

Lijin Kunjuramakurup [1], Sheik Mohammed Sulthan [2], Muhammed Shanir Ponparakkal [1], Veena Raj [3] and Mathew Sathyajith [4,*]

[1] EEE Department, TKM College of Engineering Kollam, Kerala 691005, India
[2] Faculty of Engineering, Universiti Teknologi Brunei, Bandar Seri Begawan BE1410, Brunei
[3] Faculty of Integrated Technologies, Universiti Brunei Darussalam, Bandar Seri Begawan BE1410, Brunei
[4] Faculty of Engineering and Science, University of Agder, 4879 Grimstad, Norway
* Correspondence: sathyajith.mathew@uia.no

Abstract: In this paper, a two-input, single-output (TISO) DC-DC converter for electric vehicle charging applications with solar photovoltaic (PV) as one of the sources is discussed. A novel, simple, and effective control strategy with maximum power point tracking (MPPT) to maximize power from PV while maintaining a constant bus voltage is proposed. A 100 V, 100 W TISO DC-DC converter is designed and comprehensive simulations are conducted under different conditions. The system characteristics are validated by comparing the results with a conventional P&O algorithm and multiple step size P&O algorithm. The proposed control strategy can precisely generate control signals to track MPPT while maintaining the bus voltage by controlling the output of a fixed DC source according to the changes in PV generation. The overall efficiency of the proposed approach is 98.67%, and the average output voltage is 99.09 V under selected conditions. The overall average output voltage ripple is 0.22% with the proposed approach, while it is 2.91% and 1.55% with the conventional P&O and multiple step size P&O MPPT techniques, respectively. Further, a 500 V, 17 kW high-power converter is designed and a simulation is carried out. The high-power converter provides an average output voltage of 496.92 V with an overall efficiency of 98.72%, and the average output voltage ripple is 0.16%. The results obtained from the simulation under the selected conditions lead to the conclusion that the converter has better efficiency and less variation in the output voltage at higher power levels with the proposed control technique.

Keywords: TISO converter; renewable energy sources; solar PV module; MPPT algorithms; linear line–slope interpolation algorithm

Citation: Kunjuramakurup, L.; Sulthan, S.M.; Ponparakkal, M.S.; Raj, V.; Sathyajith, M. A High-Power Solar PV-fed TISO DC-DC Converter for Electric Vehicle Charging Applications. *Energies* **2023**, *16*, 2186. https://doi.org/10.3390/en16052186

Academic Editor: Carlo Renno

Received: 2 January 2023
Revised: 17 February 2023
Accepted: 18 February 2023
Published: 24 February 2023

1. Introduction

Rising fossil fuel costs and new legislation aimed at reducing CO2 emissions in conventional vehicles have increased the interest in electric vehicles (EVs). EVs require effective charging systems to "refuel" their batteries on a regular basis for smooth and continuous operation [1,2]. The simultaneous connection of a number of EVs to the electrical grid for recharging raises the power demand and generates other grid-related issues. Utilizing renewable energy sources (RES) for the recharging of EVs is one of the solutions in resolving the power grid challenges. Solar PV power generation is superior to other renewable energy sources due to the advantages that it presents. Charging stations powered by solar PV may offer pollution-free electricity to EVs, which positively impacts the environment [3,4]. However, EV charging requires a reliable and regulated power supply for efficient charging. The irregular and random output of solar PV systems necessitates the development of hybrid energy systems (HESs) employing a reliable power source with solar PV output to provide a regulated output for EV charging applications. The sources in HES are often connected independently to the load via single- or multi-stage power electronic DC-DC

converters, which reduce the overall efficiency and are bulky. Multi-input (MI) DC-DC converters, on the other hand, provide simple circuits with lower costs and greater efficiency, and they integrate multiple energy sources to deliver power at a controlled voltage [5]. A two-input single-output DC-DC converter with solar PV as one of the power sources is discussed in this article. The following section describes the related works proposed in the literature, focusing on multi-input converters. The paper is further subdivided into sections as follows. Section 3 discusses the operation and design of the TISO DC-DC converter; Section 4 analyzes the simulation results, and Section 5 concludes the work.

2. Related Works

A three-level isolated MI converter is introduced in [6], with fewer components and less voltage stress on the power electronic components. When the converter circuit input inductors are selected appropriately, they operate in discontinuous conduction mode (DCM), allowing independent power distribution between the input sources. However, a transformer is required for insulation, resulting in an increased size and cost. Further, the DCM mode of operation requires complicated control schemes. In [7], a bidirectional DC-DC converter with a multi-input transformer for hybrid wind–PV–battery systems is presented. Wind power is captured in the proposed circuit through a half-bridge auxiliary converter coupled to a transformer. In contrast, PV energy is harnessed using a bidirectional buck–boost converter that controls battery charging and discharging. A single-phase, full-bridge bidirectional converter is used to deliver power to the loads and communicate with the grid. However, the system is more expensive because of the inclusion of three converters and a multi-winding transformer. Due to the existence of a transformer, isolated MI converters are only useful in highly demanding situations. As a result, non-isolated MI converters with a simple structure and higher energy density have gained popularity, considering their affordability.

An MI DC-DC boost converter is proposed in [8], which comprises a battery storage device and two boost converters, with an additional capacitor substituted in one of the converters. However, the proposed architecture has more components, a complicated control method, and lower efficiency. A high-voltage-gain MI converter with an inductor in a single-architecture form is presented in [9]. Here, zero voltage switching (ZVS) of two of the four primary switches and the management of the bidirectional power flow between the lower and upper sides of voltage require complex control techniques. In addition, coupled inductors and switches increase both the size and cost. A non-isolated MI DC-DC converter circuit is described in [10], which receives output power from a group of low-powered small wind turbines. The designed circuit architecture consists of two stages with a network of DC-DC converters, which leads to the need for more components and a cumbersome system. Furthermore, numerous steps in operation decrease the overall efficiency of the converter. A modular, non-isolated MI DC-DC converter without a coupled inductor is proposed in [11]. The proposed design uses fewer components to produce the appropriate voltage gain, which can lower the converter's dimensions, weight, price, and losses while increasing its efficiency. However, significant stress on the power electronic components necessitates complex control schemes for continuous-input-current operation.

Recently, [12] introduced a three-input DC-DC boost converter. It has a standard buck–boost and a boost converter with one bidirectional battery port and two unidirectional power source ports. The large number of passive and semiconductor components in the system has resulted in an increased size and cost with less efficiency. A further MISO step-up converter is introduced in [13], where the load is fed from two sources either separately or simultaneously. This structure is simple and improves the power output, power source utilization, and fault tolerance of the source. However, the switches are subjected to high voltage stress and thus operate with lower efficiency. An MI DC-DC converter based on SEPIC is presented in [14], with an initial stage that connects many input voltage sources and a battery management system (BMS) stage that allows the charging and discharging of the battery. However, during the operation of the proposed converter, the power electronic

components and diodes are subject to considerable stress. The large number of components in the system further increases the costs and reduces the efficiency. An MI buck DC-DC converter with a single inductor is proposed in [15]. While there are fewer parts, the suggested architecture may not be acceptable for high-voltage applications since the output voltage is less than the lowest input voltage. Additionally, all input diodes must be changed out for power switches to allow bidirectional operation, practically doubling the switch count, which increases the switching losses and voltage stress on switches and raises the price.

A modified double-input DC–DC converter with a bridge-type configuration, capable of integrating renewable and non-renewable sources and storage systems, is presented in [16]. In the same structure, the suggested converter will work in step-down, step-up, and step-up/down mode. The topology can supply power to the load even if one of the input sources is not available. However, a complex control system is required to drive multiple-input voltage sources simultaneously and for the bidirectional power flow. A transformer-less high-voltage-gain DC-DC MI converter is recommended in [17]. The converter combines the conventional boost and buck–boost converters. It has reduced voltage stress on the power electronic components, and a wide control range of the input sources. However, additional diodes required for the multi-input converter to work continuously increase the cost and component count. A MISO DC-DC power converter described in [18] allows communication between multiple energy sources with different power levels using a dual boost converter connected to the same DC bus. This circuit demands a complex control mechanism for its operations. S. Mohammadi et al. [19] introduced a high-voltage-gain non-isolated MI DC-DC converter, in which the load on the switches can be reduced by adding more input units and selecting a lower duty ratio for each unit. However, the requirement for numerous components makes operation costly and inefficient.

A non-isolated MI boost DC-DC converter with fewer components and higher efficiency is suggested in [20], having input sources that can supply a common load while being completely managed and running concurrently. With this structure, any voltage or current sources can be taken as the converter's input and plugged into and unplugged from the converter using a plug-and-play interface. The range of suggested converter applications in various low to high voltage and power ranges can be extended by enhancing the converter voltage gains by adding additional input sources. However, the performance of the converter is analyzed with two fixed DC sources. The benefits of this converter topology have prompted further research in the converter to determine the feasibility of incorporating solar PV as one of the sources.

In this paper, the performance of the two-input single-output DC-DC converter proposed in [20] is studied by integrating solar PV as one of the sources with a linear line–slope control technique. The study concentrates on the adoption of photovoltaic solar power to charge electric vehicles. The following are the key contributions of this article.

(i) Design of a 100 W TISO converter and implementation of a novel control strategy for MPPT tracking and voltage regulation simultaneously.
(ii) Model development of designed system with proposed controller in MATLAB/Simulink.
(iii) Analysis of output voltage stability in terms of output voltage ripple using P&O, multiple step size P&O, and proposed control approach.
(iv) Simulation and analysis of the proposed approach under various conditions.
(v) Performance analysis of a high-power converter with proposed control technique.

3. Two-Input Single-Output (TISO) DC-DC Converter

The TISO DC-DC converter circuit is shown in Figure 1a, with a variable input voltage source E_1 and a constant DC voltage source E_2. The circuit consists of two switches, S_1 and S_2; two inductors, L_1 and L_2; four capacitors, C_0, C_1, C_2, and C_3; and three diodes, D_1, D_2, and D_3. Despite the fact that the converter may function in both continuous and discontinuous conduction modes depending on the inductor current levels, this work

concentrates on the continuous conduction mode of operation. The switching waveforms and inductor current waveforms are shown in Figure 1b.

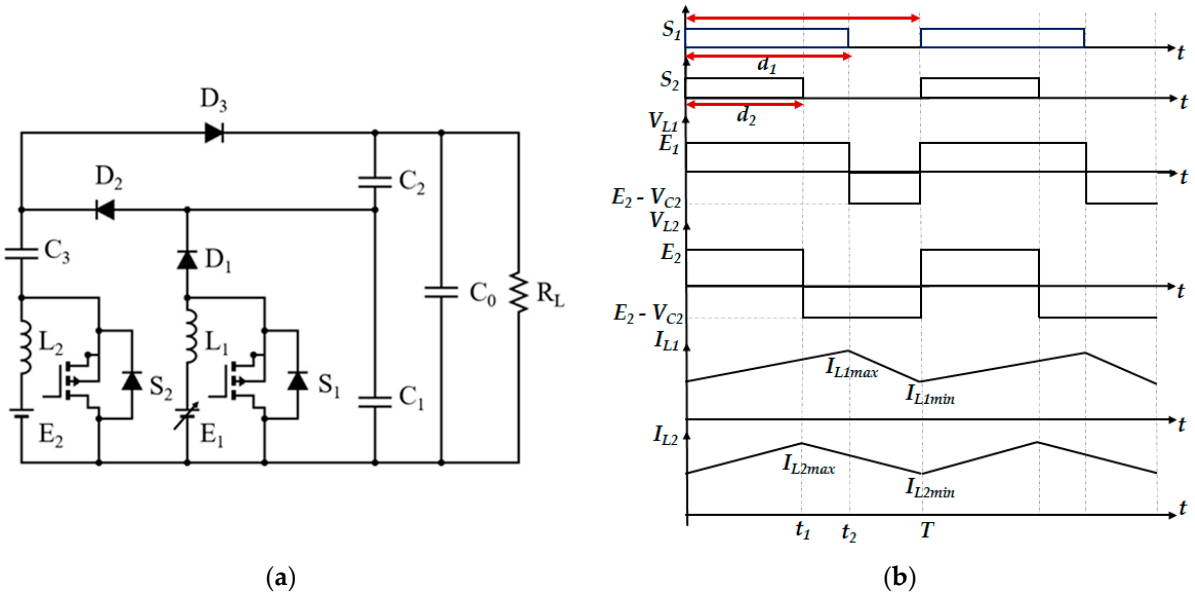

(**a**) (**b**)

Figure 1. (**a**) TISO DC−DC converter circuit. (**b**) Switching pulse and inductor current waveform of TISO DC-DC converter.

The operation of the converter circuit in continuous conduction mode (CCM) can be carried out in four different modes. In the first mode, the diodes D_1 and D_3 are reverse-biased, the diode D_2 is forward-biased, and S_1 and S_2 are switched ON, resulting in an increase in current in inductors L_1 and L_2 linearly and the discharge of capacitors C_1 and C_0 via diode D_2, charging the capacitors C_2 and C_3. This mode of operation continues until the diode D_2 is turned off as the current through the capacitor C_3 becomes zero. In the second mode, S_1 and S_2 continue in their conduction states; all diodes are reverse-biased, and switches S_1 and S_2 are conducting, while L_1 and L_2 continue to be in the charging mode, C_2, which discharges to the load. In the third mode, S_2 continues to conduct, whereas S_1 is commutated; D_3 is forward-biased, but D_1 and D_2 are reverse-biased. Due to the energy stored in L_2 and C_3, the capacitors C_1, C_2, and C_0 are charged. S_1 continues to be in the OFF state in the fourth mode, and S_2 is commutated. D_1 and D_3 are forward-biased, whereas D_2 is reverse-biased. As the two inductors and capacitor C_3 discharge, capacitors C_1, C_2, and C_0 are charged.

The TISO converter discussed here is a boost converter that provides the combined output voltage of E_1 and E_2 in the steady state. The operation of the circuit is controlled so as to supply the desired output by supplying voltages from the sources.

When S_1 is ON, $V_{L1} = E_1$, and when S_1 is OFF, $V_{L1} = E_1 - V_{C1}$.

Likewise, when S_2 is ON, $V_{L2} = E_2$; when S_2 is OFF, $V_{L2} = E_2 - V_{C2}$.

According to the inductor volt-sec balance, for E_1,

$$(E_1 \times d_1 T) + [(E_1 - VC_1) \times (1 - d_1)T] = 0 \quad (1)$$

Similarly,

$$(E_2 \times d_2 T) + [(E_2 - VC_2) \times (1 - d_2)T] = 0 \quad (2)$$

From the above equations, we obtain

$$E_1 - VC_1\,(1 - d_1) = 0 \text{ and}$$
$$E_2 - VC_2\,(1 - d_2) = 0$$

The output voltage is

$$V_0 = VC_1 + VC_2$$

Thus, the equation to calculate the converter's output voltage is given by

$$V_0 = \frac{E_1}{1-d_1} + \frac{E_2}{1-d_2} \tag{3}$$

where d_1 and d_2 are the corresponding switching ratios of the control switches S_1 and S_2, and E_1 and E_2 are the source voltages. Knowing the source voltages E_1 and E_2, by setting the desired output voltage and fixing one of the duty cycles, say d_1, another duty cycle (d_2) can be obtained. For this study, a solar PV module with V_{max} of 18 V (E_1) and a fixed DC source of 12 V (E_2) are selected. A TISO DC-DC converter is designed for E_1 = 18 V, E_2 = 12 V, output voltage (V_0) = 100 V, output voltage (P_0) = 100 W, and switching frequency f = 15 KHz. The following subsections describe the selection of the load resistance, inductor, and capacitor values.

3.1. Selection of Load Resistance

The load resistance can be obtained from

$$R_L = \frac{{V_0}^2}{P_0} \tag{4}$$

3.2. Selection of Inductor Values

To ensure the CCM mode of operation, the inductor's value should be higher than the critical value (L_k), which is given by

$$L_K = \frac{R_L(d_1 + 2\alpha d_2)(1-d_1)^2(1-d_2)^2}{2f(1+d_2-2d_1d_2)(1+\alpha(1-d_1)-d_2)} \tag{5}$$

where α is the input voltage ratio and is given by $\alpha = \frac{E_2}{E_1}$, and f is the switching frequency.

3.3. Selection of Capacitor Values

The minimum capacitor value can be calculated from

$$C_k = \frac{\lambda V_0}{f R_{L\min} V_{pp\max}} \ (k = 0,1,2,3) \tag{6}$$

The effect of the output voltage ripple is included by a factor λ. The range of λ is 1 to 3 and it is regarded as 1.6 in this study. V_{ppmax} is the output voltage ripple, which is usually assumed to be 2% of V_0. R_{Lmin} is the minimum load resistance, which is assumed to be 20% of the load resistance [21].

4. Simulation Results and Discussion

4.1. Conventional Circuit

The parameters and designed component values of the converter are listed in Table 1. Figure 2 illustrates the MATLAB/Simulink simulation model for a basic TISO DC-DC converter with two fixed 18 V and 12 V DC input voltage sources. The duty ratios d_1 and d_2 are maintained at 0.7 throughout the simulation. Figure 3a illustrates the output voltage, while Figure 3b illustrates the converter power.

Table 1. Design parameters and component values of TISO DC-DC converter.

Description	Value
Input Voltage (E_1)	18 V
Input Voltage (E_2)	15 V
Duty Ratio (d_1 and d_2)	0.7
Switching Frequency (f)	15 kHz
Output Voltage (V_0)	100 V
Output Power (P_0)	100 W
Boost Inductance (L_1 and L_2)	200 µH
Capacitance (C_0, C_1, C_2, and C_3)	267 µF
Load Resistance (R_L)	100 Ω

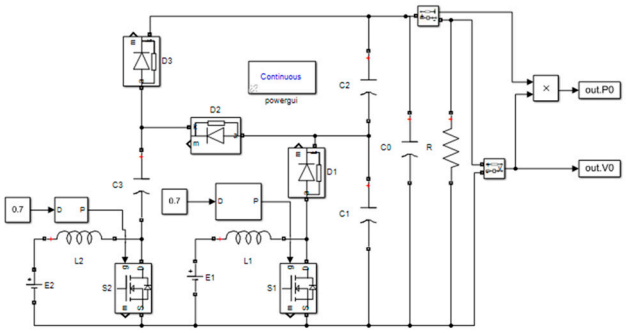

Figure 2. Basic TISO DC-DC converter Simulink model.

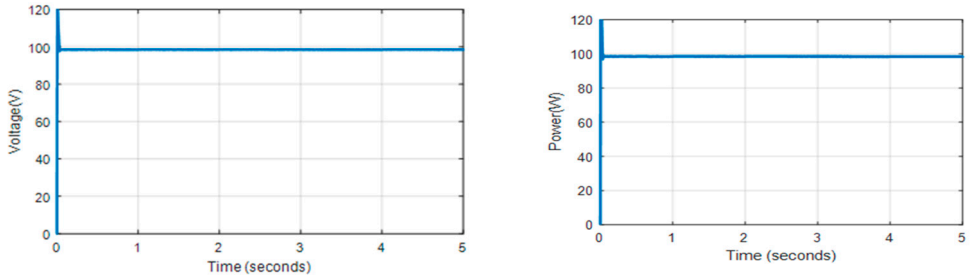

(**a**) (**b**)

Figure 3. (**a**) Converter's output voltage at constant input voltages. (**b**) Converter's output power at constant input voltages.

The average power calculated from the simulated output power curve is 98.49 W; hence, the converter efficiency is 98.49%. Using the simulation results, the voltage ripple and average output voltage are calculated to be 0.21% and 99.195 V, respectively. These figures indicate that the converter has greater efficiency and lower output voltage fluctuation. Losses due to passive components and solid-state switches influence converter efficiency. Power loss in MOSFETs is caused by conduction loss, switching loss, and body diode resistance. However, owing to the CCM mode of operation, body diode resistance losses are disregarded. Power losses due to diodes include threshold voltage loss, conduction loss, switching loss, and reverse recovery current loss, all of which are dependent on the output current, output voltage ripple, and switching frequency [20,22,23]. This study does not evaluate the influence of parasitic components such as trace inductances, parasitic capacitances, and semiconductors on efficiency computation, since this work is primarily focused on the system level rather than the component level.

Figure 4a shows the simulated waveforms of the switching pulses of switches S_1, S_2, the inductor voltage, and the inductor current. The plots show that the results are aligned with the steady−state analysis plots depicted in Figure 1b. In Figure 4b, voltages across the capacitors C_0, C_1, C_2, and C_3 are shown.

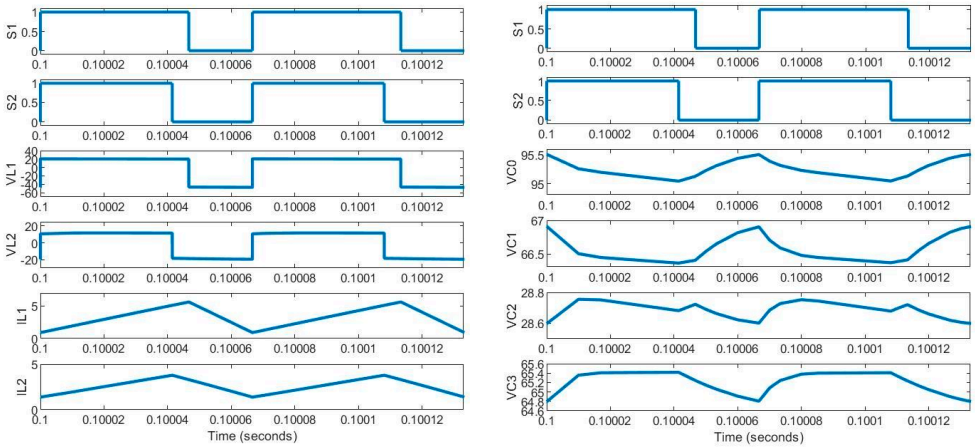

Figure 4. (**a**) Switching pulses, inductor voltage, and inductor current. (**b**) Switching pulses and capacitor voltage.

4.2. TISO DC−DC Converter with Solar PV Input

4.2.1. MPPT Tracking Algorithms

Solar photovoltaic systems are equipped with MPPT controls to ensure that they operate at MPP for optimal efficiency. A large number of MPPT technologies are proposed in the literature on solar photovoltaic systems [24]. The Perturb and Observe (P&O) method is a popular and widely recognized MPPT approach due to its simple architecture and ease of implementation in comparison to other techniques [25]. A conventional P&O MPPT has a step size of 0.01, and the algorithm gradually increases or decreases the duty ratio until the MPP is attained. The major drawbacks of the P&O method are oscillations around the MPP under steady-state conditions and slow tracking speeds in rapidly changing weather conditions. Variable-step P&O methods are introduced to address the shortcomings of the conventional P&O approach [26]. The improved multi-step P&O approach increases the tracking speed and reduces oscillations because of the multiple step sizes used for tracking. When the operating point is far from the MPP, the algorithm creates a large step value, and when the operating point is close to the MPP, it generates a small step value. Figure 5 depicts the flowchart of the multi-step P&O approach.

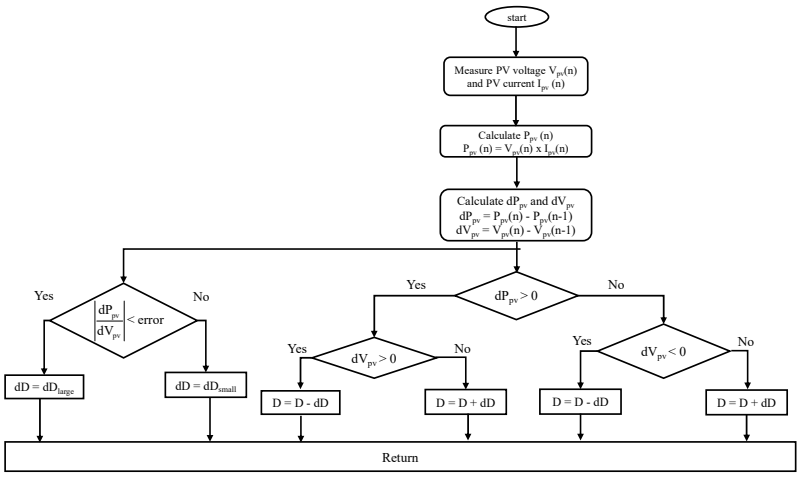

Figure 5. Flowchart of variable-step P&O MPPT algorithm [26].

4.2.2. Analysis of TISO DC-DC Converter with Solar PV

To investigate the circuit characteristics with a solar PV as one of the sources, the 18 V fixed DC source is replaced with a solar PV module with a maximum peak output voltage of 18 V, and the 12 V fixed DC source is kept as a secondary source of input voltage. Specifications of the solar PV module are listed in Table 2. The circuit is simulated with P&O and multiple-step size P&O MPPT. Figure 6 shows the MATLAB/Simulink model. Based on the output voltage of the solar PV module, the duty ratio of the switch linked to the PV module is adjusted by an MPPT controller to harvest the maximum power. Simultaneously, the controller will adjust the duty cycle of the switch connected to a fixed DC input source, to keep the output voltage constant.

Table 2. Solar PV Module Specifications.

Description	Value
Peak power (P_{max})	100 W
Voltage at peak power (V_{max})	18 V
Current at peak power (I_{MAX})	5.56 A
Short-circuit current (I_{sc})	6.06 A
Open-circuit voltage (V_{oc})	22 V
Temperature coefficient of Isc	(0.06 ± 0.15)%/°C

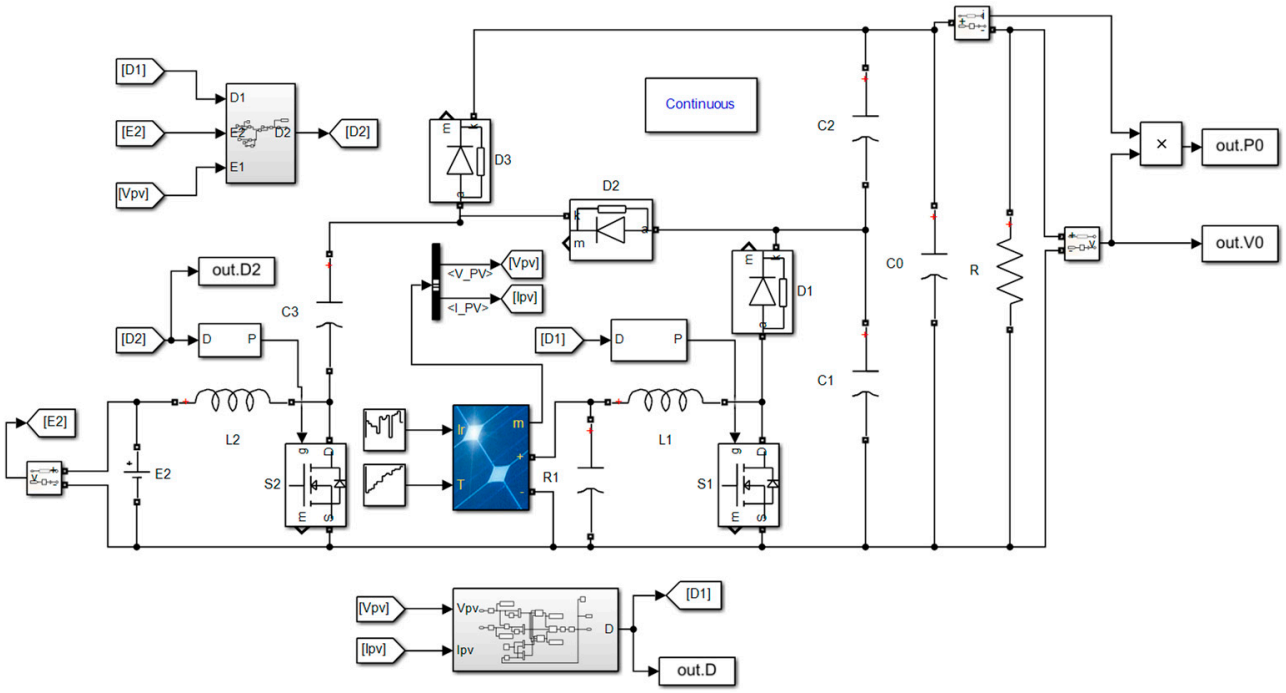

Figure 6. Solar-powered TISO DC-DC converter Simulink model.

4.2.3. Analysis under Changing Irradiation at a Constant Temperature

The circuit is simulated under various irradiance levels at a constant temperature (25 °C), as shown in Figure 7. Figure 8 depicts the change in the duty ratio of switch S_1 corresponding to the changes in PV output. Figure 9 shows the duty ratio generated by the control circuit for switch S_2 with respect to the changes. The converter's output voltage and output power are depicted in Figures 10 and 11, respectively.

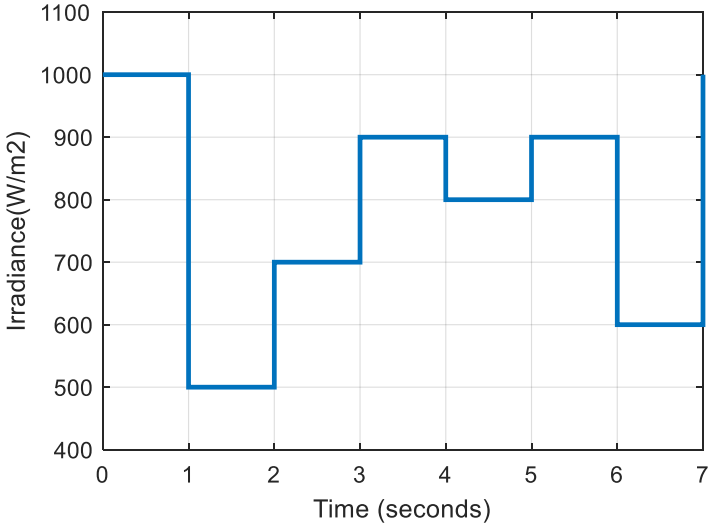

Figure 7. Variation in irradiation level.

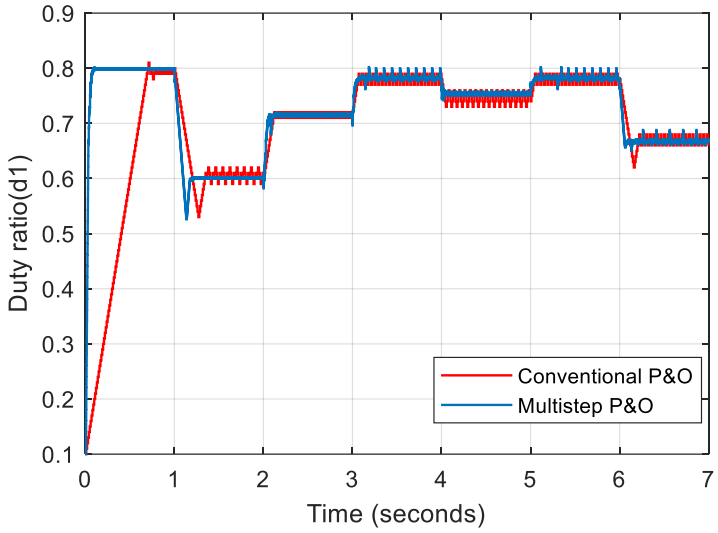

Figure 8. Duty ratio variation of S1 corresponding to different irradiation levels.

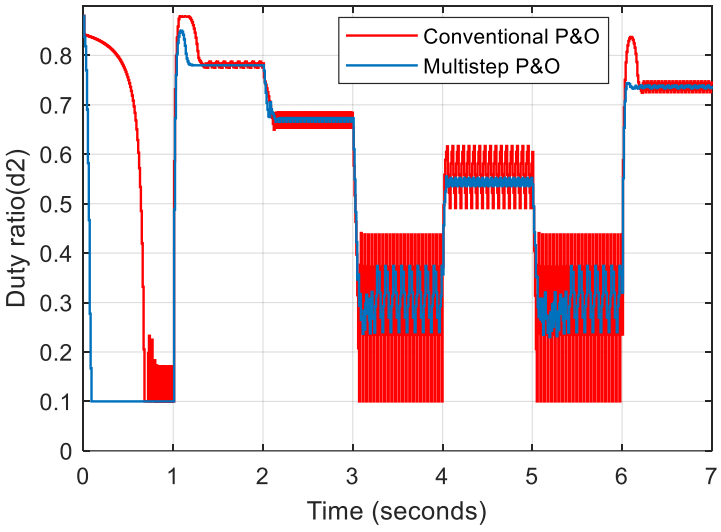

Figure 9. Duty ratio variation of S_2 corresponding to different irradiation levels.

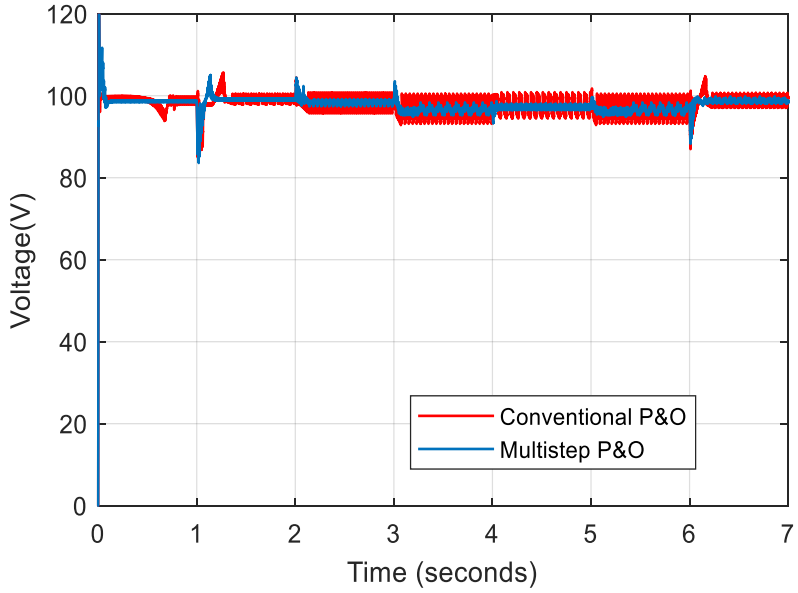

Figure 10. Converter's output voltage in various irradiation levels.

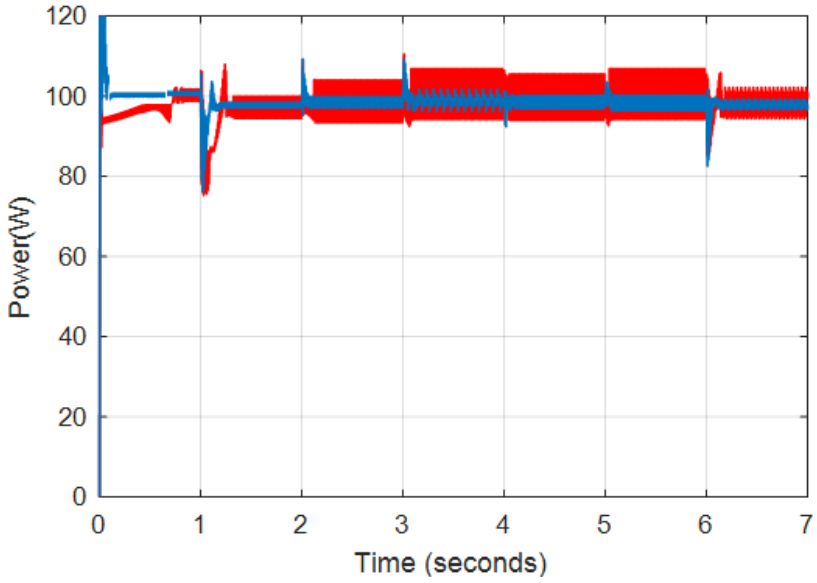

Figure 11. Converter's output power in various irradiation levels.

Table 3 displays the average voltage value and ripples in the output voltage estimated from the voltage waveform, the average power value and converter efficiency computed from the power waveform, and the time delay to achieve MPP for each MPPT method. The average voltage, voltage ripple, and overall efficiency with P&O MPPT and multiple-step-size P&O MPPT are also presented in the table. It can be seen that both methods provide almost the same average output voltage and power. However, multi-step P&O is more efficient than conventional P&O in terms of MPP tracking and output voltage ripple. Meanwhile, multiple-step-size P&O also induces ripples in the output due to duty cycle oscillation around the MPP. Since the duty cycle of the fixed source control switch completely depends on the duty cycle and output voltage of the PV modules, this causes an additional ripple in the output. Hence, using the P&O algorithm or its variant for tracking is not ideal to achieve a stable output voltage, even though they assure maximum power extraction.

Table 3. Performance comparison of the converter with P&O MPPT Algorithms.

Solar Irradiation (W/m^2)	Time Delay in Seconds		Average Output Voltage (V_{out})		Percentage of Ripple		Average Output Power (P_{out})		Efficiency (η)	
	Conv P&O	Multi P&O	Conv P&O	Multi P&O	Conv P&O	Multi P&O	Conv P&O	Multi P&O	Conv P&O	Multi P&O
1000	0.73	0.096	98.83	98.64	2.16%	1.34%	99.8	98.95	99.80%	98.95%
500	0.35	0.183	99.24	99.06	2.34%	1.56%	97.22	97.8	97.22%	97.80%
700	0.12	0.098	98.26	98.28	5.20%	1.79%	98.2	98.5	98.20%	98.50%
900	0.07	0.051	96.81	96.81	7.62%	3.26%	99.7	98.9	99.70%	98.90%
800	0.05	0.028	97.68	97.31	6.60%	1.75%	99.65	98.6	99.65%	98.60%
900	0.05	0.027	96.81	96.81	7.62%	3.26%	99.7	98.9	99.70%	98.90%
600	0.2	0.076	98.9	98.97	3.66%	1.77%	98.33	97.9	98.33%	97.90%
Overall Average			**98.87**	**98.81**	**2.91%**	**1.55%**	**99.07**	**98.43**	**99.07%**	**98.43%**

To overcome the ripple issue and to produce a more stable output, a simple indirect MPPT method with a linear line–slope interpolation algorithm is proposed. Figure 12 depicts the flowchart of the linear line–slope interpolation algorithm approach. The algorithm reads the input(s) and provides a corresponding output based on the preassigned values stored as an array. Duty ratio values are stored for each set of irradiation and temperature values for irradiation values ranging within 500:100:1200 W/m^2 and temperature values ranging within 15:10:45 °C with a constant period of 10 °C, and duty cycle values are determined. A total of 38 sets of values are stored.

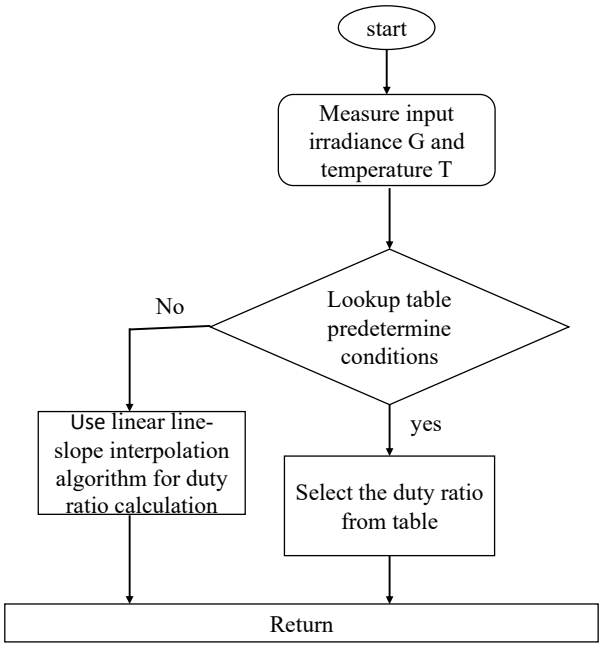

Figure 12. Flowchart of the linear line–slope interpolation algorithm.

The linear line–slope interpolation algorithm directly provides the duty ratio to the switch from the stored data, if the irradiation and temperature inputs match the stored data; otherwise, the duty ratio is calculated by the algorithm using the linear interpolation formula. The algorithm provides a constant value as output and hence the output ripple is eliminated.

$$v = v_1 + \frac{u - u_1}{u_2 - u_1} \times (v_2 - v_1) \quad (7)$$

The circuit is simulated with the proposed approach for similar input conditions applied to the P&O and multistep P&O MPPT-based system (Figure 7). Figure 13 depicts

the duty ratio generated by the linear line–slope interpolation algorithm given to switch S_1 and the duty ratio produced by the proposed control architecture for switch S_2. The voltage and power output of the converter are depicted in Figures 14 and 15, respectively.

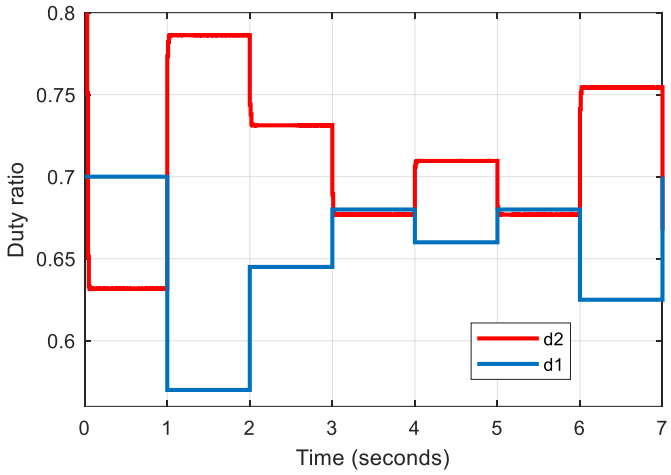

Figure 13. Duty ratio variation of S1 and S2 corresponding to different irradiation levels.

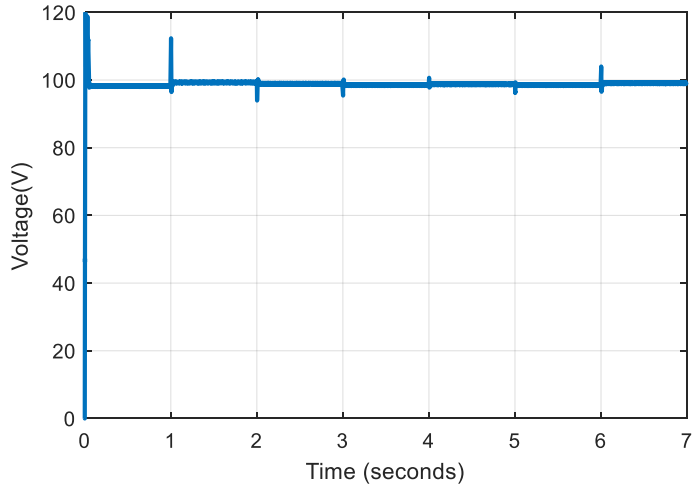

Figure 14. Output voltage of converter in different irradiation levels.

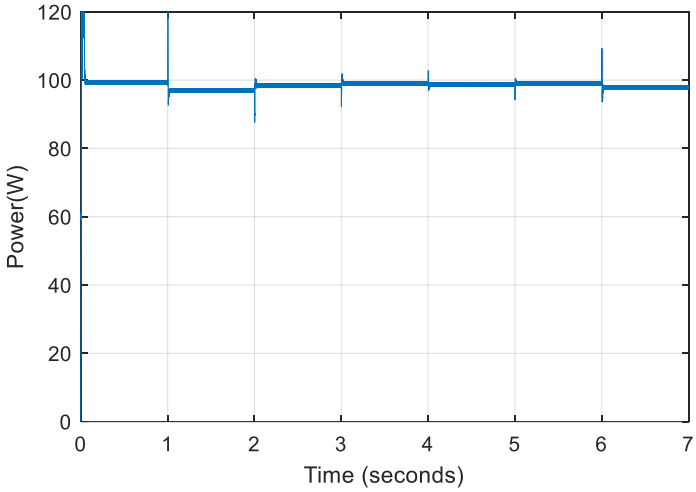

Figure 15. Converter's output power in different irradiation levels.

The duty ratios of switch S_1 vary with the variation in irradiation at a constant temperature, causing the duty ratios of switch S_2 to change due to the control topology used to maintain a constant voltage in the converter. Observations of the output power and voltage waveforms indicate that the output is comparatively more stable. Table 4 displays the average voltage and percentage output voltage ripple calculated from the voltage waveform, the average power value, and converter efficiency computed from the power waveform.

Table 4. Average output voltage, voltage ripple, average output power, and efficiency of the converter with proposed MPPT algorithm.

Solar Irradiation (W/m^2)	Average Output Voltage (V_{out})	Percentage of Ripple	Average Output Power (P_{out})	Efficiency (η)
1000	99.03 V	0.22%	98.3 W	98.30%
500	98.93 V	0.22%	97.49 W	97.49%
700	98.92 V	0.23%	98.85 W	98.85%
900	98.62 V	0.23%	99.34 W	99.34%
800	99.09 V	0.24%	99.08 W	99.08%
900	98.62 V	0.23%	99.34 W	99.34%
600	98.92 V	0.23%	98.39 W	98.39%

The average voltage and overall efficiency of the converter with the proposed controller are 98.9 V and 98.67%, respectively, and the average voltage ripple is 0.228%. It is evident from the results that the proposed approach is capable of tracking MPP much faster than the P&O tracking approach and the voltage ripple is significantly reduced. The ripple reduction is more than 90% when compared to 2.91% ripple generated by the P&O algorithm, and it is more than 85% when compared to 1.55% voltage ripple in the multiple-step-size P&O algorithm.

4.2.4. Analysis of Rapidly Changing Environmental Conditions with Real-Time Data

The effectiveness of a solar-powered DC-DC converter employing the linear line–slope interpolation technique is examined using real-time data samples where both temperature and irradiance values fluctuate dramatically. Irradiance and temperature on a specific day in the last week of April 2022 from Kollam, India (9.02 N, 76.91 E) are used for the analysis under rapidly changing environmental circumstances and are shown in Figures 16 and 17, respectively. Between 10:00 a.m. and 12:30 p.m., the irradiation varies dramatically. Fourteen data samples are collected at equal intervals between 11 a.m. and 12:20 p.m. for the analysis. Figures 18 and 19 demonstrate the fluctuations in irradiance and temperature across the given time period. Figures 20 and 21 show the changes in temperature and irradiance, which are assumed to be occurring every 10 s for simulation purposes. Figures 22 and 23 illustrate the variation in the duty ratios of switches S_1 and S_2. Figures 24 and 25 depict the generated output voltage and power, respectively.

The duty ratios of switch S_1 vary with respect to the changes in irradiation and temperature, which causes the duty ratios of switch S_2 to shift to keep the output voltage constant. The average voltage, output voltage ripples, average power, and converter efficiency computed from the simulation results are listed in Table 5.

4.2.5. Analysis of High-Power Converter

A 500 V, 17 kW high-power converter with a switching frequency of 20 kHz is designed and simulated with the proposed control approach. Here, a solar PV array with a maximum peak output voltage of 183.95 V and a power output of 11 kWp is used as a primary source. The voltage of the secondary input voltage source of the 12 V fixed DC source is fixed at 96 V. The parameters and values of the designed components of the converter are listed in Table 6, and the specifications of the solar PV array are listed in Table 7.

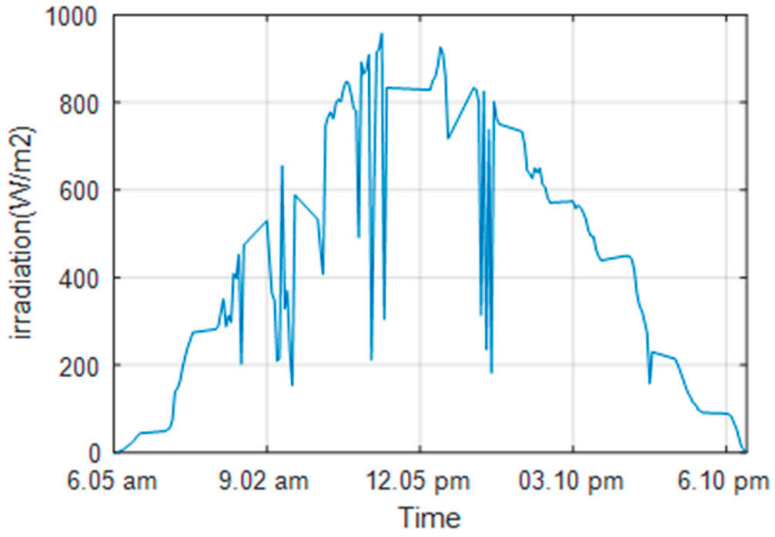

Figure 16. Rapid changes in irradiance occurring throughout the day.

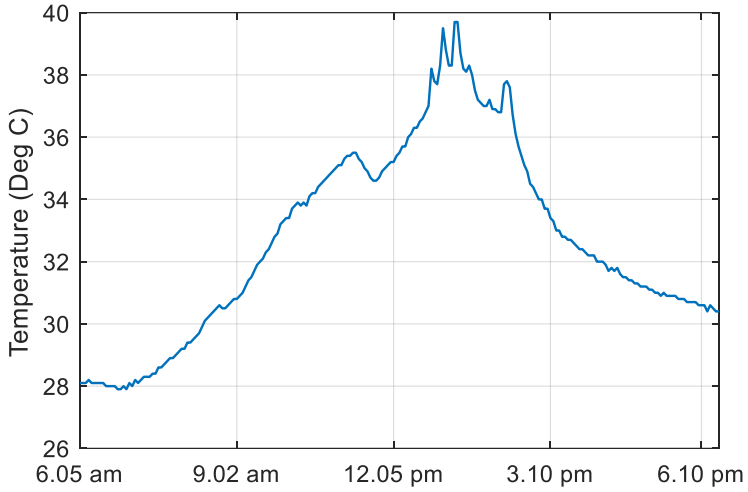

Figure 17. Rapid changes in temperature occurring throughout the day.

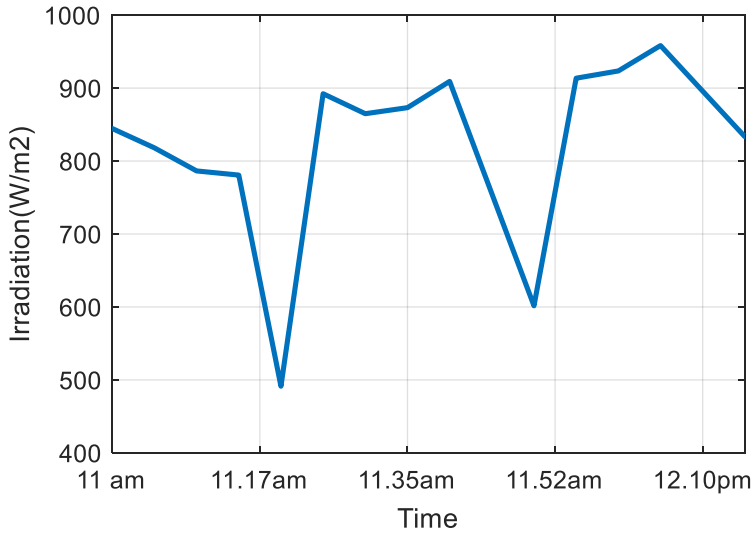

Figure 18. Irradiation data samples between 11 a.m. and 12.20 p.m.

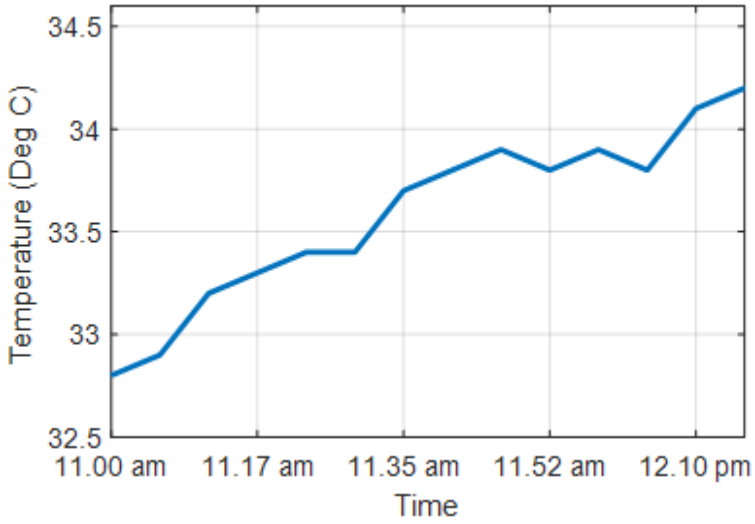

Figure 19. Temperature data samples between 11 a.m. and 12.20 p.m.

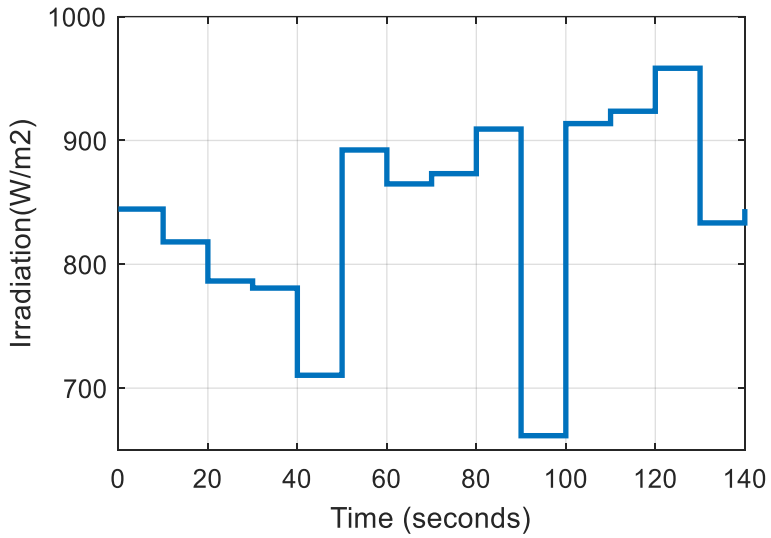

Figure 20. Rapidly changing irradiation levels for simulation.

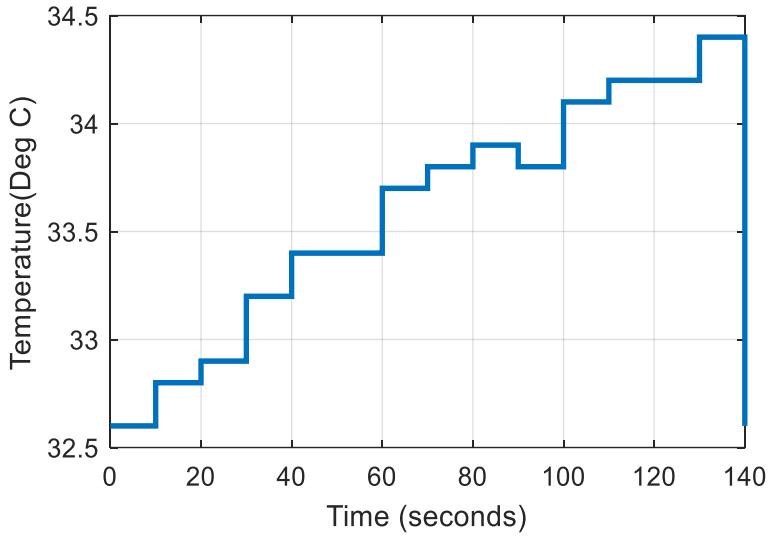

Figure 21. Rapidly changing temperature levels for simulation.

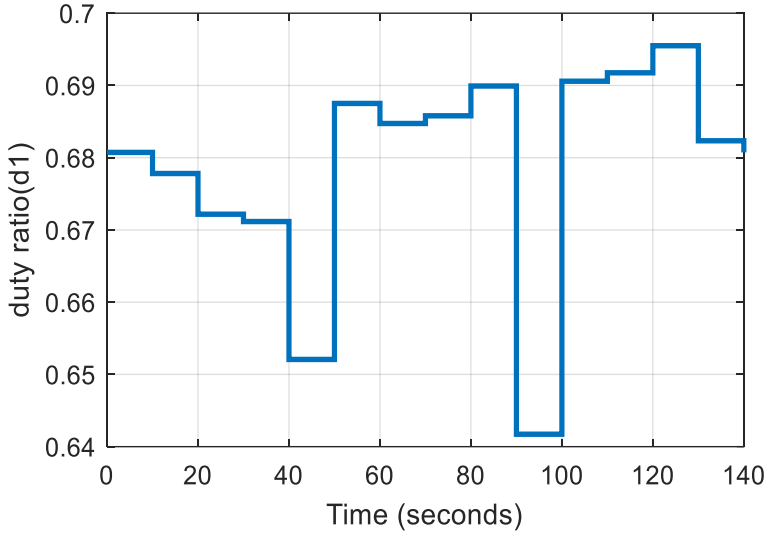

Figure 22. Duty ratio variation of S_1 under rapidly varying conditions.

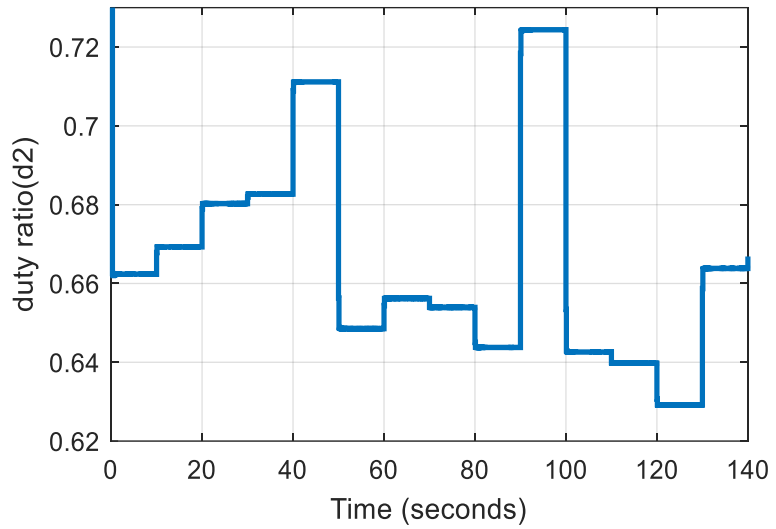

Figure 23. Duty ratio variation of S_2 under rapidly varying conditions.

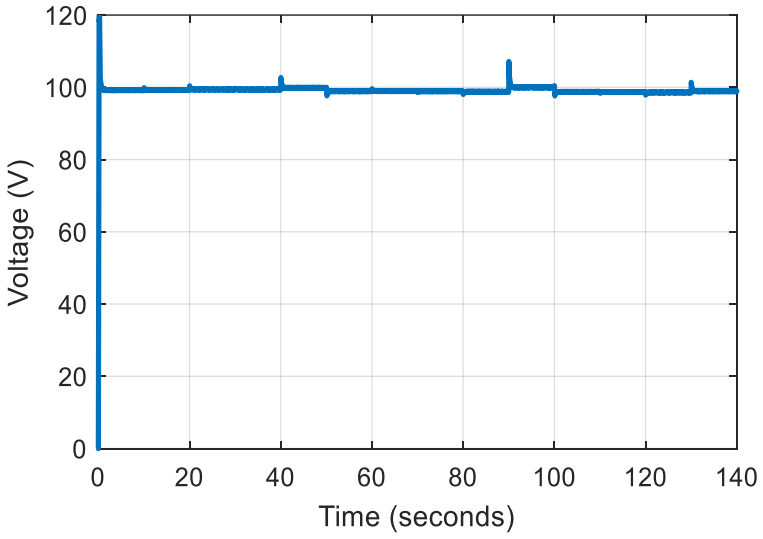

Figure 24. Output voltage of the low power TISO converter under rapidly varying conditions.

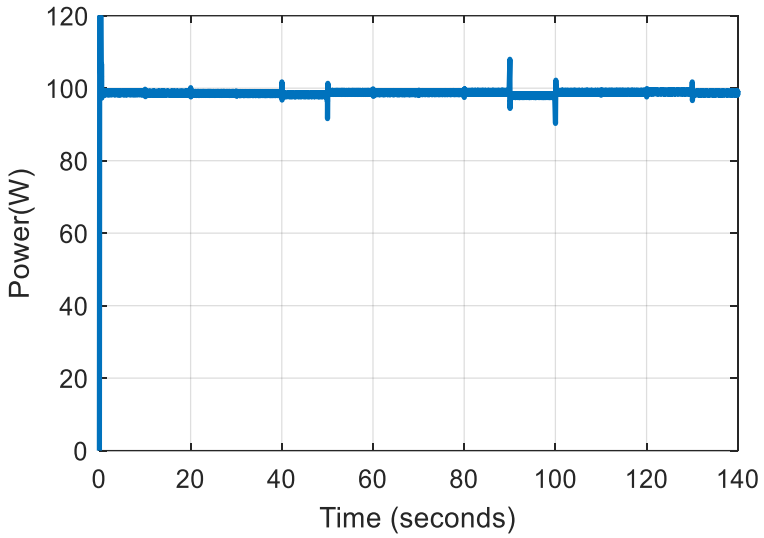

Figure 25. Output power of the TISO converter under rapidly varying conditions.

Table 5. TISO converter analysis under rapidly varying PV inputs.

Irradiation (W/m^2)	Temperature (°C)	Average Output Voltage (V_{out})	Percentage of Ripple	Average Output Power (P_{out})	Efficiency (η)
844.6	32.8	99.21 V	0.22%	98.73 W	98.73%
818.1	32.9	99.25 V	0.23%	98.65 W	98.65%
786.5	33.2	99.4 V	0.22%	98.65 W	98.65%
780.8	33.4	99.39 V	0.23%	98.51 W	98.51%
710.4	33.4	99.87 V	0.22%	98.18 W	98.18%
892.3	33.7	98.92 V	0.22%	98.83 W	98.83%
864.9	33.8	98.95 V	0.23%	98.77 W	98.77%
873.2	33.8	98.91 V	0.22%	98.83 W	98.83%
909.2	33.9	98.78 V	0.22%	98.86 W	98.86%
661.6	33.8	99.72 V	0.24%	97.95 W	97.95%
913.6	34.1	98.74 V	0.22%	98.86 W	98.86%
923.6	34.2	98.69 V	0.22%	98.89 W	98.89%
958.3	34.2	98.57 V	0.2%	98.96 W	98.96%
833.4	34.4	98.91 V	0.22%	98.67 W	98.67%
Overall average		**99.09 V**	**0.22%**	**98.67 W**	**98.67%**

Table 6. Specifications of High power TISO DC-DC converter.

Description	Value
Input Voltage (E_1)	180 V
Input Voltage (E_2)	96 V
Duty Ratio (d_1)	0.5
Duty Ratio (d_2)	0.314
Switching Frequency (f)	20 kHz
Output Voltage (V_0)	500 V
Output Power (P_0)	17 kW
Boost Inductance (L_1 and L_2)	100 µH
Capacitance (C_0, C_1, C_2, and C_3)	1359.6 µF
Load Resistance (R_L)	14.71 Ω

Table 7. Solar PV array specifications.

Description	Value
Peak power (P_{max})	220 W
Voltage at peak power (V_{max})	36.79 V
Current at peak power (I_{max})	5.98 A
Short-circuit current (I_{sc})	6.31 A
Open-circuit voltage (V_{oc})	45.31 V
Number of parallel strings	10
Number of series connected per string	5
Temperature coefficient of Isc	$(0.06 \pm 0.15)\%/^{\circ}C$

The circuit simulation is performed under the rapidly changing environmental conditions presented in Section 4.2.3 as input for the PV array. Figures 26 and 27 illustrate the variation in the duty ratios of switches S_1 and S_2. Figures 28 and 29 depict the generated output voltage and power, respectively.

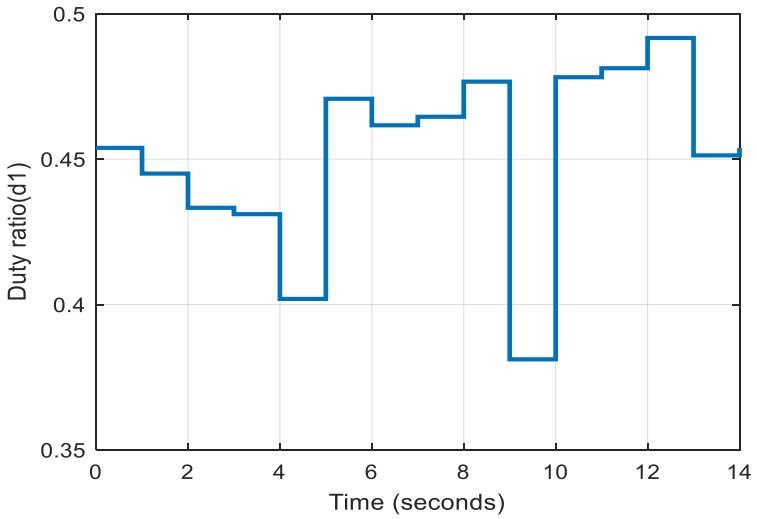

Figure 26. Duty cycle of switch S_1 of the high-power converter under rapidly varying PV inputs.

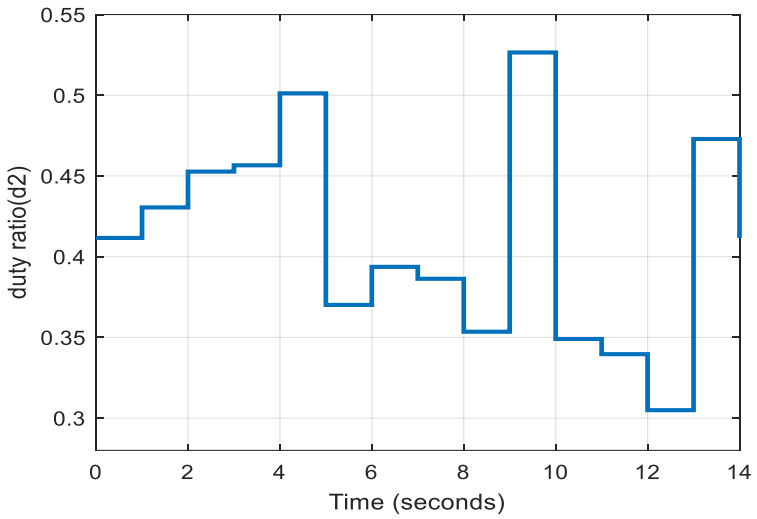

Figure 27. Duty cycle of switch S_2 of the high-power converter under rapidly varying PV inputs.

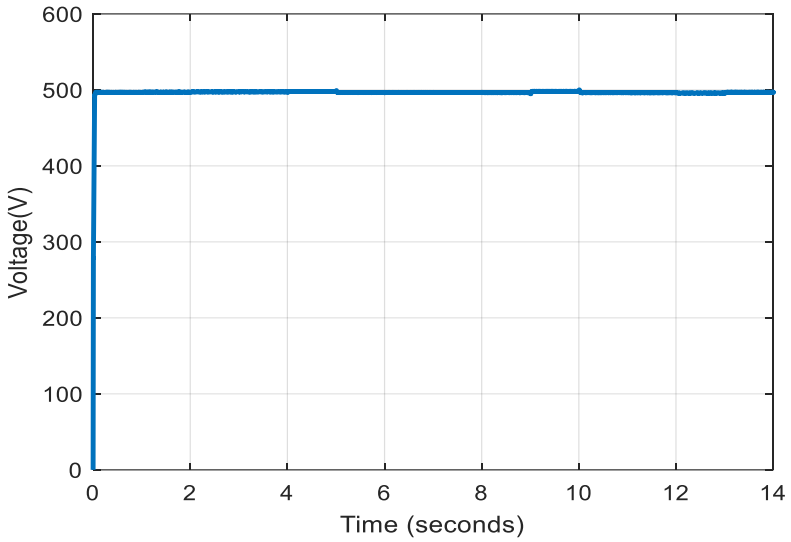

Figure 28. Output voltage of the high-power converter under rapidly varying PV inputs.

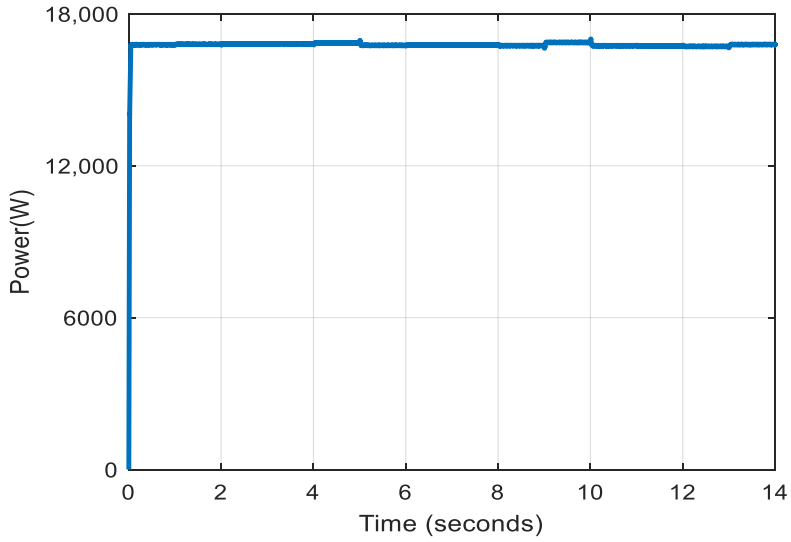

Figure 29. Output power of the high-power converter under rapidly varying PV inputs.

The performance of the circuit is found to be satisfactory since the output voltage is almost constant throughout the simulation period, irrespective of the variations in the PV input, and the output power is also very close to the expected value. The average voltage, output voltage ripples, average power, and converter efficiency calculated from the simulation results are given in Table 8.

The high-power converter provides an average output voltage of 496.92 V. The overall efficiency of 98.72% and average ripple percentage of 0.16% obtained from the simulation under the selected conditions lead to the conclusion that the converter has better efficiency and less variation in the output voltage under higher power levels with the proposed control technique. When the MPP operation of a solar photovoltaic system is compromised and it is unable to achieve a constant output voltage, the developed converter with the linear line–slope interpolation approach offers better efficiency and less variation in the output voltage. More specifically, the output voltage ripple is significantly reduced, which reduces the filter size of the converter system, the size, and the cost.

Table 8. The average output voltage, voltage ripple, average output power, and efficiency of the high-power converter under rapidly varying PV inputs.

Irradiation (W/m^2)	Temperature (°C)	Average Output Voltage (V_{out})	Percentage of Ripple	Average Output Power (P_{out})	Efficiency (η)
844.6	32.8	496.9 V	0.16%	16.785 kW	98.74%
818.1	32.9	497.1 V	0.16%	16.8 kW	98.82%
786.5	33.2	497.35 V	0.14%	16.815 kW	98.91%
780.8	33.4	497.35 V	0.14%	16.815 kW	98.91%
710.4	33.4	498.3 V	0.16%	16.855 kW	99.15%
892.3	33.7	496.5 V	0.16%	16.755 kW	98.56%
864.9	33.8	496.7 V	0.16%	16.775 kW	98.68%
873.2	33.8	496.6 V	0.16%	16.77 kW	98.65%
909.2	33.9	496.3 V	0.16%	16.745 kW	98.50%
661.6	33.8	498.2 V	0.16%	16.86 kW	99.18%
913.6	34.1	496.3 V	0.16%	16.745 kW	98.50%
923.6	34.2	496.4 V	0.16%	16.735 kW	98.44%
958.3	34.2	495.9 V	0.16%	16.715 kW	98.32%
833.4	34.4	497 V	0.16%	16.795 kW	98.79%
Overall average		**496.92 V**	**0.16%**	**16.783 kW**	**98.72%**

5. Conclusions

A two-input single-output DC-DC converter with solar PV as one of the sources is presented and discussed in this paper. A liner line–slope interpolation method is proposed for solar PV power extraction. A detailed analysis of a 100 V, 100 W DC-DC converter circuit with a 12 V fixed DC source and 18 V solar PV module as sources is carried out through simulation studies under various conditions. The circuit characteristics in terms of output voltage, power, efficiency, and voltage stability are evaluated by comparing the converter's results with the proposed approach against the conventional P&O MPPT and multiple-step-size P&O MPPT algorithms. With the proposed approach, the converter offers overall efficiency of 98.67% and the overall output voltage of the converter is 99.09 V. The proposed approach significantly reduces the ripple generated in the output voltage. The output voltage ripple is 0.22%, which is much lower than with the other approaches. A 500 V, 17 kW TISO DC-DC converter with a 180 V, 11 kWp solar PV array and a 96 V fixed DC source is also designed and simulated under different input conditions by varying the solar PV input. The obtained results are promising as the converter provides an overall average output of 496.92 V at 98.72% efficiency. The output voltage ripple is only 0.16%. The results confirm the feasibility of integrating a solar PV module as one of the sources with the proposed technique for a TISO converter for EV charging applications.

Author Contributions: Conceptualization, L.K. and S.M.S.; methodology, L.K., S.M.S. and M.S.P.; software, L.K. and S.M.S.; validation, L.K., S.M.S., M.S.P., V.R. and M.S.; formal analysis, L.K., S.M.S. and M.S.P.; writing—original draft preparation, L.K. and S.M.S.; writing—review and editing, L.K., S.M.S., M.S.P., V.R. and M.S.; funding: M.S. All authors have read and agreed to the published version of the manuscript.

Funding: The authors would like to acknowledge the University of Agder, Norway, for providing financial assistance for the publication of this article.

Conflicts of Interest: The authors declare no conflict of interest.

References

1. Adib, A.; Shadmand, M.B.; Shamsi, P.; Afridi, K.K.; Amirabadi, M.; Fateh, F.; Ferdowsi, M.; Lehman, B.; Lewis, L.H.; Mirafzal, B.; et al. E-Mobility-Advancements and Challenges. *IEEE Access* **2019**, *7*, 165226–165240. [CrossRef]
2. Mohammed, S.S.; Ahamed, T.I.; Aleem, S.H.A.; Omar, A.I. Interruptible Charge Scheduling for Plug-In Electric Vehicle to Minimize Charging Cost Using Heuristic Algorithm. *Electr. Eng.* **2021**, *104*, 1425–1440. [CrossRef]
3. Titus, F.; Thanikanti, S.B.; Deb, S.; Kumar, N.M. Charge Scheduling Optimization of Plug-In Electric Vehicle in a PV Powered Grid-Connected Charging Station Based on Day-Ahead Solar Energy Forecasting in Australia. *Sustainability* **2022**, *14*, 3498. [CrossRef]
4. Affam, A.; Buswig, Y.M.; Othman, A.-K.B.H.; Bin Julai, N.; Qays, O. A review of multiple input DC-DC converter topologies linked with hybrid electric vehicles and renewable energy systems. *Renew. Sustain. Energy Rev.* **2020**, *135*, 110186. [CrossRef]
5. Reddy, K.J.; Natarajan, S. Energy sources and multi-input DC-DC converters used in hybrid electric vehicle applications–A review. *Int. J. Hydrogen Energy* **2018**, *43*, 17387–17408. [CrossRef]
6. Dusmez, S.; Li, X.; Akin, B. A new multiinput three-level DC/DC converter. *IEEE Trans. Power Electron.* **2015**, *31*, 1230–1240. [CrossRef]
7. Mangu, B.; Akshatha, S.; Suryanarayana, D.; Fernandes, B.G. Grid-Connected PV-Wind-Battery-Based Multi-Input Transformer-Coupled Bidirectional DC-DC Converter for Household Applications. *IEEE J. Emerg. Sel. Top. Power Electron.* **2016**, *4*, 1086–1095. [CrossRef]
8. Ahrabi, R.R.; Ardi, H.; Elmi, M.; Ajami, A. A Novel Step-Up Multiinput DC-DC Converter for Hybrid Electric Vehicles Application. *IEEE Trans. Power Electron.* **2016**, *32*, 3549–3561. [CrossRef]
9. KhademiAstaneh, P.; Javidan, J.; Valipour, K.; Akbarimajd, A. A bidirectional high step-up multi-input DC-DC converter with soft switching. *Int. Trans. Electr. Energy Syst.* **2018**, *29*, e2699. [CrossRef]
10. Majeed, Y.E.; Ahmad, I.; Habibi, D. A Multiple-Input Cascaded DC-DC Converter for Very Small Wind Turbines. *IEEE Trans. Ind. Electron.* **2018**, *66*, 4414–4423. [CrossRef]
11. Varesi, K.; Hosseini, S.H.; Sabahi, M.; Babaei, E. A high-voltage gain nonisolated noncoupled inductor based multi-input DC-DC topology with reduced number of components for renewable energy systems. *Int. J. Circuit Theory Appl.* **2017**, *46*, 505–518. [CrossRef]
12. Kardan, F.; Alizadeh, R.; Banaei, M.R. A New Three Input DC/DC Converter for Hybrid PV/FC/Battery Applications. *IEEE J. Emerg. Sel. Top. Power Electron.* **2017**, *5*, 1771–1778. [CrossRef]
13. Dhananjaya, M.; Pattnaik, S. Design and Implementation of a Multi-Input Single-Output DC-DC Converter. In Proceedings of the 1st IEEE International Conference on Sustainable Energy Technologies and Systems (ICSETS), Bhubaneswar, India, 26 February–1 March 2019; pp. 194–199. [CrossRef]
14. Haghighian, S.K.; Tohidi, S.; Feyzi, M.R.; Sabahi, M. Design and analysis of a novel SEPIC-based multi-input DC/DC converter. *IET Power Electron.* **2017**, *10*, 1393–1402. [CrossRef]
15. Varesi, K.; Hosseini, S.H.; Sabahi, M.; Babaei, E.; Vosoughi, N. Performance and design analysis of an improved non-isolated multiple input buck DC-DC converter. *IET Power Electron.* **2017**, *10*, 1034–1045. [CrossRef]
16. Athikkal, S.; Sundaramoorthy, K.; Sankar, A. Design, fabrication and performance analysis of a two input-single output DC-DC converter. *Energies* **2017**, *10*, 1410. [CrossRef]
17. Banaei, M.R.; Ardi, H.; Alizadeh, R.; Farakhor, A. Non-isolated multi-input-single-output DC/DC converter for photovoltaic power generation systems. *IET Power Electron.* **2014**, *7*, 2806–2816. [CrossRef]
18. Erdal Irmak, N.G. Application of a boost based multi-input single-output DC/DC converter. In Proceedings of the 2017 IEEE 6th International Conference on Renewable Energy Research and Applications (ICRERA), San Diego, CA, USA, 5–8 November 2017; pp. 955–961.
19. Mohammadi, S.; Dezhbord, M.; Babalou, M.; Azizkandi, M.E.; Hosseini, S.H. A New Non-Isolated Multi-Input DC-DC Converter with High Voltage gain and Low Average of Normalized Peak Inverse Voltage. In Proceedings of the 2019 10th International Power Electronics, Drive Systems and Technologies Conference (PEDSTC), Shiraz, Iran, 12–14 February 2019; pp. 515–520. [CrossRef]
20. Deihimi, A.; Mahmoodieh, M.E.S.; Iravani, R. A new multi-input step-up DC–DC converter for hybrid energy systems. *Electr. Power Syst. Res.* **2017**, *149*, 111–124. [CrossRef]
21. Liu, S.-L.; Liu, J.; Mao, H.; Zhang, Y.-Q. Analysis of operating modes and output voltage ripple of boost DC-DC converters and its design considerations. *IEEE Trans. Power Electron.* **2008**, *23*, 1813–1821. [CrossRef]
22. Gorecki, P. Electrothermal Averaged Model of a Diode–IGBT Switch for a Fast Analysis of DC–DC Converters. *IEEE Trans. Power Electron.* **2022**, *37*, 13003–13013. [CrossRef]
23. Górecki, K.; Detka, K. Influence of Power Losses in the Inductor Core on Characteristics of Selected DC–DC Converters. *Energies* **2019**, *12*, 1991. [CrossRef]
24. Mohammed, S.S.; Devaraj, D.; Ahamed, T.I. Learning Automata and Soft Computing Techniques based Maximum Power Point Tracking for Solar PV Systems. In *Intelligent Paradigms for Smart Grid and Renewable Energy Systems*; Springer: Berlin/Heidelberg, Germany, 2020.

25. Mohammed, S.S.; Devaraj, D.; Ahamed, T.I. A Novel Hybrid Maximum Power Point Tracking technique using Perturb & Observe Algorithm and Learning Automata for solar PV system. *Energy* **2016**, *112*, 1096–1106.
26. John, R.; Mohammed, S.S.; Zachariah, R. Variable step size Perturb and observe MPPT algorithm for standalone solar photovoltaic system. In Proceedings of the 2017 IEEE International Conference on Intelligent Techniques in Control, Optimization and Signal Processing (INCOS), Srivilliputtur, India, 23–25 March 2017; pp. 1–6. [CrossRef]